Available online at www.sciencedirect.com
SCIENCE DIRECT®
Thin Solid Films 496 (2006) 520 – 525
thin solid films
www.elsevier.com/locate/tsf

Dielectric modeling of transmittance spectra of thin ZnO:Al films

Zhaohui Qiao [a], Chitra Agashe [b], Dieter Mergel [a,*]

[a] Physics Department, WG Thin Film Technology, University Duisburg-Essen, 45117 Essen, Germany
[b] Institut für Photovoltaik, Forschungszentrum Jülich, 52425 Jülich, Germany

Received 18 February 2004; received in revised form 27 July 2004; accepted 17 August 2005
Available online 15 September 2005

Abstract

A dielectric model comprising band gap transitions and free electron excitations (Drude model) is successfully applied to simulate transmittance spectra of ZnO films doped with 0.5%, 1% and 2% Al. The Drude formula contains a frequency-dependent damping term in order to get a good fit in the visible spectral region. Useful physical parameters obtained from the fit are electron density and mobility within the grains, film thickness, band gap and refractive index. The optically determined film thickness agrees with that obtained with the stylus method within 2%. The optically determined electronic parameters are compared with those obtained by electrical measurements. Contrary to thin In_2O_3:Sn films, the Drude mobility inside the grains is similar to the direct current Hall mobility indicating more perfect film growth without forming pronounced grain boundaries. Maximum value is 35 cm^2/V s. The effective electron mass is estimated to be about 0.6 of the free electron mass. The refractive index at 550 nm decreases with increasing electron density.

PACS: 71.20.Nr; 78.20.Bh; 73.61
Keywords: Zinc oxide (563); Electrical properties (112); Optical properties (345)

1. Introduction

Transparent conductive oxides (TCOs) refer to a class of materials in thin film form which possess simultaneously high transparency in the visible wave length range, high reflectance in the infrared range along with a good electrical conductivity of nearly semi-metallic regime. This combination of physical properties makes TCOs widely applicable in a variety of optoelectronic devices where one makes use of either the optical and electrical properties, or both of them, as e.g. for transparent electrodes.

Thin films based on SnO_2, In_2O_3 and ZnO with a moderate concentration of oxygen vacancies form this class of n-type semiconductors. These materials doped with cations (In_2O_3:Sn [1,2] and ZnO:Al [3]) or anions (SnO_2:F [4]) yield improved degenerate n-type semiconductors. ZnO based TCOs like ZnO:Al are especially attractive as compared to In_2O_3- and SnO_2-based TCOs since they promise cost-effectiveness, due to the relative abundance of Zn. Further, the technological applicability of ZnO:Al based TCOs has well been established in recent years, for example as a standard front contact in solar cells based on amorphous silicon as well as in a variety of other thin film solar cells [5,6].

The free carrier absorption and high infrared reflectivity in the infrared spectral region are mainly decided by the carrier concentration N, whereas the steepness of the change-over from high transparency in the visible to the minimum transparency for higher wave lengths is governed by the carrier mobility [2,7,8]. Hence, to tailor the optical properties of a good TCO, one needs to tailor the electrical transport parameters as well. A theoretical analysis of experimentally obtained optical properties like the transmittance and reflectance of these films can be used to deepen the understanding of their properties. Such efforts have been successfully employed earlier for In_2O_3:Sn [2,8,9] and ZnO:Al [10,11] films. These approaches characterise the optical properties of the thin films by devising a complex dielectric function, $\varepsilon = f(\lambda)$ with a corresponding complex refractive index $n = \varepsilon^{1/2}$ that, together with the knowledge of the film thickness, is able to reproduce the experimentally observed spectra. In earlier work, the film thickness was determined independently and the theoretical transmittance was calculated from a hypothetical ε that was

* Corresponding author. Tel.: +49 201 183 2551; fax: +49 201 183 4242.
E-mail address: dieter.mergel@uni-essen.de (D. Mergel).

0040-6090/$ - see front matter © 2005 Elsevier B.V. All rights reserved.
doi:10.1016/j.tsf.2005.08.282

varied directly at every wave length observing continuity constraints but not assuming specific physically justified formulas [2]. In another paper, ε was calculated by use of the Drude formula for the excitations of free electrons and the fit was obtained only in a limited spectral region, e.g. in the infrared for $\lambda > 0.6$ μm in order to evaluate the plasma edge [11].

Recently, dielectric modeling was used by our group to generate theoretical spectra for the transmittance and reflectance of thin In_2O_3:Sn films in the spectral range from 200 to 2000 nm where both the band gap and the plasma edge occur [8]. In order to get a satisfying fit, the following models were applied to derive the dielectric function:

(1) A harmonic oscillator to represent the inter-band transitions into the upper half of the conduction band. This is a rough approximation that does not take into account the details of the band structure. It is, however, sufficient for the spectral range of the transmittance spectra ($E < 4$ eV) that is far below the critical points of the combined density of states.
(2) A modified Drude model with frequency-dependent damping to describe the intra-band transitions of the electrons in the conduction band. The frequency-dependent damping is necessary to get a good fit to the experimental spectrum in the visible range. It is a computational novelty and can be justified by energy-dependent scattering of electrons at ionized donors [2].
(3) The O'Leary–Johnson–Lim (OJL) model that has been proposed to model the band gap transitions of amorphous silicon [12]. This model is chosen for practical purposes — it yields a good fit to the spectra and contains only four parameters: the band gap energy, the decay energy to describe an exponential tail extending into the band gap and two amplitudes. In the case of ITO, we have tried more complicated models including direct and indirect optical transitions. Since these models did not yield more useful information, we decided to use the simpler OJL model instead [8].

In the present contribution, we investigate whether these models are applicable to thin films of ZnO:Al.

2. Experimental details

ZnO:Al films with different extent of Al doping were prepared at the Institut für Photovoltaik (IPV), Forschungszentrum Jülich by radio frequency (RF) magnetron sputtering using oxidic targets (ZnO/Al_2O_3) with an Al_2O_3 content of 0.5, 1 and 2 wt.%. The diameter of the target is 6 in. The RF sputter power was 225 W. The substrate was heated to a fixed temperature of 100 °C. For all experiments, a mixture of argon and oxygen was introduced to the chamber with a flux ratio of 7 : 0.1 sccm yielding a sputtering pressure of 0.27 Pa (2 mTorr). The deposition rate is in the range of 0.40–0.55 nm/s. The influence of the various sputter parameters on the physical properties is already discussed in detail [13].

The geometrical thickness was measured in the uniformity zone of the films with the stylus method by a Dektak apparatus. The transmittance spectra were recorded in the spectral range from 200 to 2200 nm with a Perkin Elmer spectrometer. The measured transmittance curves can be simulated and fitted based on the dielectric modeling performed with a commercial computer program [14]. From the optical spectra simulation, film thickness, free carrier density and mobility, band gap and refractive index of the films can also be obtained [8]. The resistance was measured with a four-point probe. The direct current (DC) electrical parameters, electron density and mobility, were determined with the Hall effect in van der Pauw geometry using a Keithley 926 Hall setup. The electrical properties of thin ZnO:Al films prepared with these methods are described in detail in Ref. [15].

3. Results and discussion

Three types of films prepared with different Al doping were analyzed in detail. The parameters for these samples, the electrical properties derived from the four-point probe and Hall effect measurements and the film thickness obtained by stylus profilometry are summarized in Table 1. From the table it is seen that the free electron density N_e^H, as derived from the Hall effect, increases from 2.9×10^{20} to 7.4×10^{20} cm^{-3} as the Al doping degree in the target increases from 0.5 to 2 wt.%. On the contrary, the free electron mobility μ_H decreases slightly from 31 to 24 cm^2/V s with increasing Al doping degree. The electrical resistivity ρ derived from the electron density n and the mobility μ ($\rho = 1/ne\mu$) also decreases with increasing doping level, which reflects that the electron density plays the main role.

The transmittance spectra of the three samples are represented in Fig. 1 together with the corresponding simulated curves. The simulated curves are shown as gray dotted lines inside the experimental spectra. It is seen that the fitting is nearly perfect. As described in the introduction in detail, the simulation of the spectra was performed with a dielectric model consisting of a Drude term, a standard band edge model (OJL model) and a harmonic oscillator to account for inter-band transitions. The parameters of the samples derived from the simulation, the band gap E_g, the optically active free carrier density N_e^{opt} and mobility μ_{opt}, the corresponding electrical resistivity ρ_{opt}, the refractive index n at 550 nm and the film thickness are listed in Table 2.

Table 1
Electrical characteristics of the films together with the thickness as obtained with stylus profilometry

Target doping	R_{sh}	ρ	N_e^H	μ_H	d_{styl}
%	Ωsq.	10^{-4} Ω cm	10^{20} cm^{-3}	cm^2/V s	nm
0.5	16	7.0	2.9	31	730
1	10.1	4.9	4.2	30	660
2	7.5	3.5	7.4	24	720

The accuracy of the parameters as obtained by repeated measurements on the same sample are: thickness d_{styl}: ±20nm, carrier density N_H: approximately ±3%, mobility: ±6%.

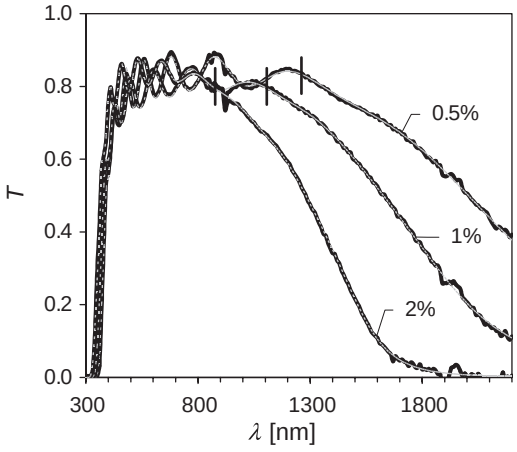

Fig. 1. Transmittance spectra of thin films (thick line) obtained from the target with 0.5, 1 and 2 wt.% Al doping degree together with the simulated spectrum (thin dashed line). The simulated curve is shown as a gray dotted line inside the recorded spectrum, because the calculated curve matches the experimental one. The Drude frequency is marked by vertical bars.

In order to get a better fit to the curvature of the plasma edge, a frequency-dependent damping factor with four fit parameters was introduced that was already successful for ITO films [8]. A frequency-dependent damping term in a Drude description was explained in terms of ionized impurity scattering [2]. One of the parameters is the Drude frequency Ω_{Dr}. Theoretically, this frequency is given by

$$\Omega_{\mathrm{Dr}}^2 = \frac{e^2 N_{\mathrm{e}}^{\mathrm{opt}}}{\varepsilon_0 m_{\mathrm{eff}}} \tag{1}$$

where $N_{\mathrm{e}}^{\mathrm{opt}}$ is the optically active free electron density, m_{eff} is the effective mass of electrons at the bottom of the conduction band, e is the elementary charge and ε_0 is the vacuum permittivity. In Fig. 1, it is indeed observed that the Drude frequency increases with increasing doping level in accordance with the plasma edge shifting towards smaller wave lengths.

The Drude model does not distinguish between the electron densities derived from the Hall effect and those active in optical transitions, i.e. $N_{\mathrm{e}}^{\mathrm{H}} = N_{\mathrm{e}}^{\mathrm{opt}}$. However, such a distinction has to be made because the experimental conditions to determine the densities are different: a direct current is used in Hall measurements and a high-frequency current in optical measurements. Furthermore, to evaluate $N_{\mathrm{e}}^{\mathrm{opt}}$ from Ω_{p}, the effective mass has to be known. In the literature, Eq. (1) is used vice versa to determine the effective mass when the Drude frequency and the free electron density are known from optical and Hall measurements, respectively. Therefore, in Fig. 2 the square of the Drude frequency is plotted against the electrically derived free electron density for the three samples.

Fig. 2 provides a possibility to check whether the assumptions of the Drude model, expressed in Eq. (1) are valid in the cases discussed here. Eq. (1) predicts a linear relationship that is indeed observed. From the slope of the trend line for our data, 1.5×10^{13}, $m_{\mathrm{eff}} = 0.6\ m_{\mathrm{e}}$ is obtained, where m_{e} is the free electron mass. The values for the data of the other authors is $0.5\ m_{\mathrm{e}}$ and $1.02\ m_{\mathrm{e}}$. Contrary to Eq. (1), the trend lines do not pass through the origin of the coordinate system. A possible explanation is given below.

The abscissa in Fig. 2 displays the electron density $N_{\mathrm{e}}^{\mathrm{H}}$ determined from the direct current Hall coefficient. For its evaluation, a formula is used that is strictly valid only for electrically homogeneous samples. Yet, the data points in Fig. 2 are obtained on polycrystalline films where the current has to pass through crystallites and, possibly extended and badly conducting, grain boundaries. The direct current conductance will be determined by the number of carriers able to cross the boundary and $N_{\mathrm{e}}^{\mathrm{H}}$ is smaller than the electron density within the crystallites.

The ordinate in Fig. 2 displays the square of the Drude frequency that, according to Eq. (1), is proportional to the electron density. The high frequency current generated by the optical excitation does not have to pass through the grain boundaries. It is representative of the electron density and mobility within the crystallites.

The difference in these two methods may explain why the optically determined parameters are generally bigger than the electrically determined parameters and why ordinate offsets are observed in Fig. 2. The data in Fig. 2 are obtained by various authors on different sets of films. They all show an ordinate offset indicating that the microstructure discussed above is important. This may be the reason why the apparent value of the effective mass, determined from the slope of the straight lines fitted to the data, is so different from one study to another.

Table 2
Optically derived characteristics of the films

Target doping	$N_{\mathrm{e}}^{\mathrm{opt}}$	μ_{opt}	n	E_0	d_{opt}	$d_{\mathrm{opt}}/d_{\mathrm{styl}}$
%	10^{20} cm^{-3}	cm^2/V s	(at 550 nm)	(eV)	nm	
0.5	4.2	35	1.95	3.37	720	0.99
1	5.5	31	1.89	3.51	650	0.985
2	8.8	36	1.80	3.72	735	1.021

The accuracy of the parameters is estimated as: refractive index n: ±0.02, electron density N_{e}: ±15%, mobility μ_{opt}: ±15%. The band gap energy is the main parameter of the OJL model.

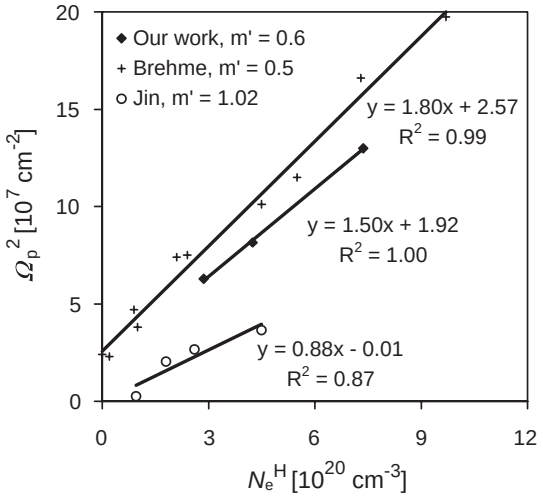

Fig. 2. Square of the Drude frequency vs. free electron density determined from the Hall coefficient. $m' = m_{\mathrm{eff}}/m_{\mathrm{e}}$. The linear fit to our data yields $m' = 0.6$.

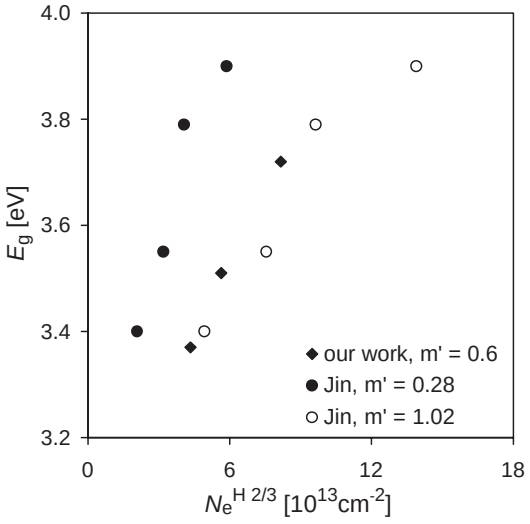

Fig. 3. Band gap E_g as derived from the OJL model vs. free carrier density. $m' = m_{eff}/m_e$.

Our value is significantly larger than the effective electron mass m_{eff}=0.28 m_e of non-degenerate bulk ZnO [16]. For comparison, the data from the work of Brehme et al. [11] and Jin et al. [10] are also plotted in Fig. 2. The slope of the trend line for the data of Brehme et al. yields an effective mass of m_{eff}=0.5 m_e. The data of Jin et al. give an even larger value of m_{eff}=1.02 m_e. Although the number of our samples is small, the derived effective electron mass is comparable with the result of Brehme et al. [11]. As discussed above, all reported values have to be regarded with caution, as the fit lines do not pass through zero contrary to Eq. (1).

The optically determined free carrier density and mobility listed in Table 2 are calculated with m_{eff}=0.6 m_e. It is seen that the optically derived values are larger than those derived by the electrical method for both the free carrier density and carrier mobility. The values are similar for the target doping with 0.5% and 1% indicating that no strong segregation takes place during the deposition, which cannot be excluded for 2% doping. In the case of ITO, the optically derived parameters were even a factor of about 1.5 to 2 larger than the DC parameters indicating that a considerable segregation with formation of badly conducting grain boundaries occurred. This discrepancy between the optically and electrically determined parameters may be explained by the polycrystalline nature of the thin films, see above the discussion of Fig. 2.

A potential explanation for the discrepancies between ITO and ZnO:Al may be the different crystalline texture of the two sets of films. The polycrystalline ITO films comprise grains of various crystalline orientations relative to the substrate normal which may generate extended grain boundaries [8]. The ZnO:Al films investigated here consist of crystallites with hexagonal crystal structure and with their *c*-axis perpendicular to the substrate [13]. This may be correlated with thin small-angle grain boundaries. Therefore, we suppose that the grain boundaries in ZnO:Al do not represent such a big obstacle to the direct electrical current as in the case of ITO. More experiments to confirm this hypothesis are needed, e.g. measuring the temperature dependence of the Hall effect and performing annealing experiments, as e.g. discussed in Ref. [17].

The optically determined mobility of ZnO:Al films is nearly a factor of three smaller than that of In_2O_3:Sn films, where values up to 90 cm^2/V s were found [8]. Brehme et al. [11] have also compared the optically determined carrier mobility with that determined by Hall effect measurements. Their observation is qualitatively in accordance with our results but their mobility is much smaller (2–10 cm^2/V s).

Fig. 3 shows the band gap as a function of the free carrier density for our samples and some results from the literature. It is observed that the band gap increases with increasing carrier density, i.e. doping level, corresponding to the shift of the Fermi level within the conduction band. For parabolic bands a linear dependence on $N_H^{2/3}$ is expected from the Burstein–Moss theory [18]. This is approximately observed. The band gap of our three ZnO:Al cases ranges from 3.4–3.7 eV, which is smaller than that for ITO films (E_g=3.80 eV) with a similar carrier density. There is also a deviation between our band gaps and the results of Jin et al [10]. However, it should be noted that Jin et al. derived the free carrier density with m_{eff}=0.28 m_e. If the effective electron mass is taken the same as for our samples or the even larger value derived from Fig. 2, then the deviation becomes much smaller.

The dielectric functions of the three samples are shown in Fig. 4. The imaginary part of the dielectric function, ε_2, can in principle be derived theoretically from the quantum mechanical electron transition probabilities and the combined density of states [19]. This is not done here but we use this relationship to discuss the main features of the dielectric function with reference to the band model.

The contributions of the three parts of our model to the total value of ε_2 (imaginary component) are locally confined and clearly separated on the wave length scale. The steep increase below 400 nm is due to the band gap transitions described by the OJL model. The soft increase starting at about 800 nm is due to the intra-band transitions of free electrons (Drude term).

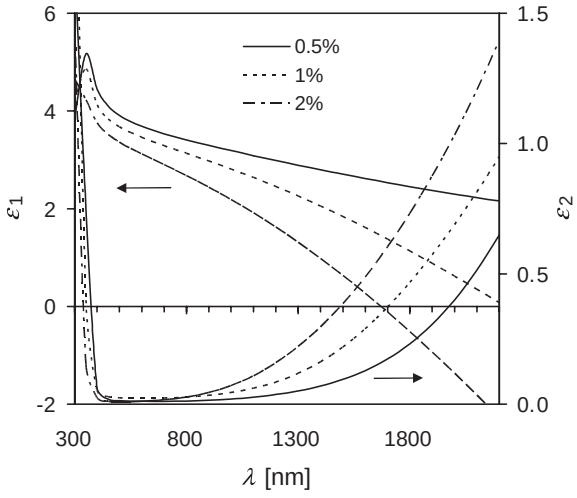

Fig. 4. Dielectric functions of the three samples.

The harmonic oscillator is positioned at 122 nm and does not contribute to ε_2 above 300 nm.

In contrast to ε_2, the individual contributions to ε_1 (real component) overlap in the whole wave length range. This is demonstrated in Fig. 5 showing ε_1 of sample "1%" together with the susceptibilities of the three contributions and is explained by the Kramers–Kronig transformation which relates the value of ε_1 at a particular wave length to the complete function of ε_2 over the whole wave length range. The susceptibility of the Drude term is negative and is responsible for the decrease of ε_1 of the samples with increasing wave length. The OJL part gives rise to the strong dispersion when λ approaches the band gap. The contribution of the harmonic oscillator is nearly wave length independent. It determines the size of ε_1 around 700 nm where the other two components cancel each other.

In order to model the inter-band transitions, we have used two mathematical models:

(a) The OJL model, designed to describe the optical transitions in the band gap region. Its main parameters are the band gap energy E_0 and the characteristic energy, γ, of the exponential band tail. E_0 and γ are found to be 3.51 eV (=354 nm) and 0.16 eV, respectively.
(b) A harmonic oscillator to describe the combined density of states for energies much larger than E_0. In the case of Fig. 5, its position is at 10.2 eV with a half-width of about 0.8 eV. To take just one harmonic oscillator is certainly a crude model, however, good enough to describe the contributions outside the range where ε_2 of this model is important.

With increasing electron density, the band gap shifts to smaller wave lengths (Burstein–Moss shift) and the intra-band transitions become stronger (corresponding to the shift of the plasma edge to smaller wave lengths). The decrease of ε_1 with increasing electron density (Fig. 4) is, therefore, a direct consequence of the apparent shifts of the band gap and the plasma wave length.

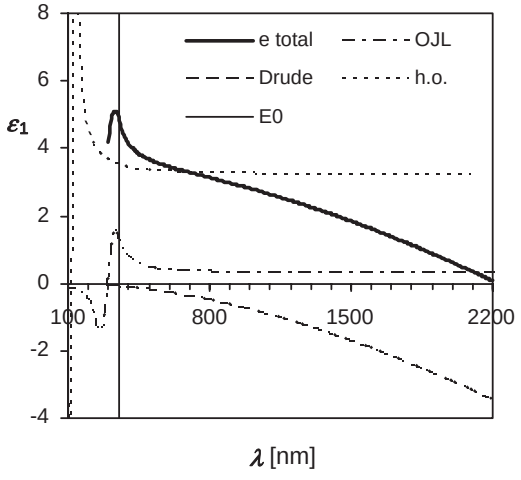

Fig. 5. Real part of the dielectric function of sample "1%" together with the individual contributions of the Drude model, the OJL model of the band gap transitions and the harmonic oscillator (h.o.) modeling the high-energy inter-band transitions. The vertical line indicates the lower limit of the experimental spectra.

The optical constants n and k are derived from the square root of ε. The refractive index n at 550 nm is roughly the same as that for ITO films with the same electron density. It is found that the refractive index decreases with increasing carrier density similar to the case of ITO films:

$$n = 2.04(2) - 0.032(3) \times 10^{-20}\left[\mathrm{cm}^3\right] N_{\mathrm{Dr}}. \quad (2)$$

The numbers in the brackets are the errors in the last digit. Comparing Eq. (2) with Eq. (16) of Ref. [8], it is found that for ZnO:Al the refractive index decreases more strongly with increasing carrier density than that for ITO films. However, further studies are needed on this. The reason for the decrease of n is the shift of both the plasma frequency and the band gap to higher energies with increasing carrier density.

In order to check the quality of the simulation, the optically determined film thickness, d_{opt}, is compared with that obtained from profilometry, d_{styl}, because these two methods are based on completely different physical principles. The ratio of these two thicknesses, $d_{\mathrm{opt}}/d_{\mathrm{styl}}$, is shown in Table 2. It is seen that the optically and geometrically determined film thicknesses are identical within 2%. This indicates that the simulation is quite reliable.

4. Conclusions

A dielectric model comprising inter-band transitions and free electron intra-band excitations is used to simulate transmittance spectra of thin ZnO:Al films. The free electron transitions are modeled by a modified Drude formula with frequency-dependent damping. The frequency-dependent damping is first of all a computational technical feature necessary to obtain a satisfactory fit to the experimental data. It is physically explained by frequency-dependent scattering at ionized donors.

Useful physical parameters obtained from the model are electron density and mobility within the grains, film thickness and refractive index. The optically determined film thickness agrees with that obtained with the stylus method within 2% indicating the reliability of the optical model.

The method itself is not new. It was already successfully applied to describe the optical properties of thin In_2O_3:Sn films. It is now used to obtain the dielectric functions for ZnO films with various contents of Al. The results for ZnO:Al are, however, sometimes different. Similar to ITO, the refractive index decreases with the electron density, due to the Burstein–Moss shift of the band edge and the stronger free electron absorption. Different to ITO, the optically determined mobility is similar to the direct current Hall mobility, at least for low doping levels. This may be a consequence of the more perfect growth of ZnO:Al films that contain only c-axis oriented grains with hexagonal crystal structure. We suppose that in such a microstructure the grain boundaries do not form such strong obstacles for the direct electrical current as in ITO films.

The effective electron mass, as obtained from a comparison of the Drude frequencies with the electron density obtained from the Hall effect, is found to be about 0.6 of the free electron mass. This confirms one of the controversial values reported in the literature. However, all reported values have to be regarded with caution as the fit lines to the experimental data, the slope of which yield the effective mass, do not pass through the origin of the coordinate system, contrary to what is expected theoretically. We suppose that this is an effect of the inhomogeneous microstructure of the films on the Hall effect.

Acknowledgements

The optical part of this work was prepared in the framework of the Graduiertenkolleg 689 “Reactivity in the surface-area” of the Deutsche Forschungsgemeinschaft. We thank O. Kluth and B. Rech of the Institut für Photovoltaik, Forschungszentrum Jülich, for fruitful discussions.

References

[1] G. Frank, H. Köstlin, Appl. Phys. A 27 (1982) 197.
[2] I. Hamberg, C.G. Granqvist, J. Appl. Phys. 60 (11) (1986) R123.
[3] H.L. Hartnagel, A.L. Dawar, A.K. Jain, C. Jagadish, Semiconducting Transparent Thin Films, Institute of Physics, London, 1995.
[4] C. Agashe, S.S. Major, J. Mater. Sci. Lett. 15 (1996) 497.
[5] B. Rech, O. Kluth, T. Repmann, T. Roschek, J. Springer, J. Mueller, F. Finger, H. Stiebig, H. Wagner, Sol. Energy Mater. Sol. Cells 74 (2002) 439.
[6] T. Nakada, Y. Hirabayashi, T. Tokado, D. Ohmori, T. Mise, Sol. Energy 77 (2004) 739.
[7] K.L. Chopra, S. Major, D.K. Pandya, Thin Solid Films 102 (1983) 1.
[8] D. Mergel, Z. Qiao, J. Phys. D: Appl. Phys. 35 (2002) 794.
[9] C.H.L. Weijtens, P.A.C. van Loon, Thin Solid Films 196 (1991) 1.
[10] Z.C. Jin, I. Hamberg, C.G. Granqvist, J. Appl. Phys. 64 (1988) 5117.
[11] S. Brehme, F. Fenske, W. Fuhs, E. Nebauer, M. Poschenrieder, B. Selle, I. Sieber, Thin Solid Films 342 (1999) 167.
[12] S.K. O’Leary, S.R. Johnson, P.K. Lim, J. Appl. Phys. 82 (1997) 3334.
[13] C. Agashe, O. Kluth, J. Hüpkes, U. Zastrow, B. Rech, M. Wuttig, J. Appl. Phys. 95 (2004) 1911.
[14] Scout 98, M. Theiss, Hard and Software for Optical Spectroscopy, Dr. Bernhard-Klein-Str. 110, 52078 Aachen, Germany, www.mtheiss.com.
[15] C. Agashe, O. Kluth, G. Schöpe, H. Siekmann, J. Hüpkes, B. Rech, Thin Solid Films 442 (2003) 167.
[16] H. Weiss, M. Schulz, O. Madelung (Eds.), Numerical Data and Functional Relationships in Science and Technology Landoldt-Börnstein New Series, vol. 17b, Springer-Verlag, Berlin, 1982, p. 35.
[17] J.E. Morris, M.I. Ridge, C.A. Bishop, R.P. Howson, J. Appl. Phys. 51 (1980) 1847.
[18] J.I. Pankove, Optical Processes in Semiconductors, Dover Pub., New York, 1971.
[19] H. Ibach, H. Lüth, Solid-State Physics, 3rd edition, Springer-Verlag, Berlin, 2003, Chapter 11.